DOI 10.1007/s11595-015-1105-x

Facile Hydrothermal Synthesis of Plasmonic Photocatalyst Ag@AgCl and Degradative Photocatalysis under Visible Light Irradiation

LIANG Yinghua, LIN Shuanglong, LIU Li, HU Jinshan, CUI Wenquan*

(Hebei Provincial Key Laboratory of Inorganic Nonmetallic Materials, College of Chemical Engineering, Hebei United University, Tangshan 063009, China)

Abstract: We put forward a new approach for the synthesis of Ag@AgCl plasmonic photocatalyst via a hydrothermal-deposition-photoreduction method. The cetylmethylammonium chloride (CTAC) was used alone as both a source of reactants and surfactant. The structure of the prepared photocatalyst was determined by XRD, SEM, EDX and UV-Vis spectroscoscopy. The photocatalytic properties were investigated by degradation of an organic pollutant, Rhodamine B, under visible light irradiation. The results reveal that the experimental conditions have a great effect on the morphology of Ag@AgCl crystals. Ag@AgCl crystal is cubic and the Ag@AgCl sample which is photoreduced for 40 min exhibits the highest photoactivity, and 80.6 % RhB is degraded after irradiation for 2 hours using this catalyst. The high photocatalytic activity observed is attributed to the surface plasmon resonance effect of Ag nanoparticles.

Key words: Ag@AgCl; hydrothermal; plasmonic photocatalyst; degradation

1 Introduction

Advanced oxidation technology using semiconductor photocatalysts has attracted increasing attention over the past two decades as an effective technique for the mineralization of pollutants of concern in air and water[1-5]. It is an emerging research topic for harvesting abundant and renewable sunlight in energy production and environmental remediation. Indeed, research on solar-driven heterogeneous photocatalysis based on surface plasmon resonance has seen rapid growth and potentially opens a technologically promising avenue that can benefit the sustainable development of global energy and the environment[6,7]. Among various photocatalytic materials, Ag@AgCl is a visible light plasmonic photocatalyst which has recently attracted considerable attention because of its high visible light absorption and activity due to the localized surface plasmon resonance (LSPR) of noble metal nanoparticles[8,9]. Recently, Huang et al. synthesized highly efficient Ag@AgCl plasmonic photocatalysts by forming AgCl powder and subsequently reducing a portion of the Ag^+ ions to Ag^0 species[10]. Various structures of Ag@AgCl photocatalysts, including microrods, irregular balls, and hollow spheres, have been successfully synthesized in the literature[11]. Yiqun Zhu *et al*[12] reported an efficient method for the synthesis of Ag@AgCl nanoparticles by an ion-exchange reaction between HCl and as-prepared Ag_2MoO_4, followed by photoreduction of Ag ions in the surface region of the prepared AgCl nanowires. Xu and co-workers[13] fabricated Ag@AgCl photocatalysts via an ionic liquids process, and Yanqing Yang *et al*[14] synthesized efficient Ag@AgCl photocatalysts using a facile deposition-photoreduction method. However, these approaches are all time-consuming and expensive, limiting the practical applications of plasmon-induced photocatalysis. Alternatively, chemical methods have been proposed for the synthesis of Ag@AgCl materials[15,16], of which the hydrothermal method is

(Received: Oct. 19, 2013; Accepted: Nov. 8, 2014)

LIANG Yinghua (梁英华): Prof.; Ph D; E-mail: liangyh@heuu.edu.cn

*Corresponding author: CUI Wenquan (崔文权): Prof.; Ph D; E-mail:wkcui@163.com

Funded partly by the National Natural Science Foundation of China (Nos. 51172063, 51202056, 51372068), Hebei Natural Science Funds for Distinguished Young Scholar (No. B2014209304), Hebei Natural Science Funds for the Joint Research of Iron and Steel (No. B2014209314), and Hebei Provincial Foundation for Returned Scholars

promising due to its good scale-up potential and strong control over structure and morphology of the prepared photocatalysts. Juan Liao *et al*[17] first reported the synthesis of efficient Ag@AgCl photocatalysts using the hydrothermal method. Ag@AgCl crystals of pure heart-like, and a mixture of heart-like and cubic shape structures were obtained by adjusting the hydrothermal parameters. In this paper, we further investigate the hydrothermal method for the synthesis of Ag@AgCl, employing cetylmethylammonium chloride (CTAC) as both a source of reactants and surfactant. Cetylmethylammonium chloride (CTAC) is a common surfactant used in hydrothermal syntheses of various nanoparticles. To the best of our knowledge, the hydrothermal synthesis of Ag@AgCl using CTAC as reactants and surfactant has not yet been reported. In the presence of CTAC, the number of nucleation sites for AgCl was thought to increase, resulting in a more homogenous dispersion of AgCl, which is desirable for the photocatalytic activity and leads to an improvement in the photocatalytic degradation observed.

2 Experimental

2.1 Synthesis of photocatalysts

All chemicals were in reagent grade and used without further purification. Ag@AgCl was synthesized via a hydrothermal-deposition-photoreduction method. 3.39 g cetylmethylammonium chloride (CTAC) and 1.5 g $AgNO_3$ were initially dissolved in 60 mL deionized water under magnetic stirring at room temperature for 30 min. After the initial mixing, the solution was transferred into a 90 mL Teflon-lined autoclave and subsequently heated in an oven. The white products obtained were successively washed by distilled water and anhydrous ethanol. The obtained AgCl powder was dispersed in 50 mL distilled water, and irradiated with a 250 W metal halide lamp (Philips). The resulting sample was then thoroughly washed with distilled water and anhydrous ethanol to remove the surfactant. The final products were dried at 80 ℃ for 8 h in the dark. The as-prepared catalysts were denoted as H-Ag@AgCl (where H is hydrothermal).

For comparison, Ag@AgCl was synthesized via a precipitation method. 3.39 g cetylmethylammonium chloride (CTAC) and 1.5 g $AgNO_3$ were initially dissolved in 60 mL deionized water under magnetic stirring at room temperature for 30 min. After that, the white products were washed by distilled water and anhydrous ethanol, respectively, and the obtained AgCl powder was dispersed in 50 mL distilled water and irradiated with a 250 W metal halide lamp (Philips). The resulting sample was then thoroughly washed with distilled water and anhydrous ethanol to remove surfactant. The final products were dried at 80 ℃ for 8 h in the dark. The as-prepared catalysts were denoted as P-Ag@AgCl (where P is precipitation).

2.2 Characterization of the photocatalysts

The crystal structure and the phase of the samples were determined by an X-ray diffractometer (XRD) using a Rigaku D/MAX2500 PC diffractometer with Cu Kα radiation, with an operating voltage of 40 kV and an operating current of 100 mA. The morphology of the samples was detected using a scanning electron microscope (SEM) (Hitachi, s-4800) and energy dispersive X-ray spectroscopy (EDX). UV-visible light (UV-vis) diffuse reflectance spectra were recorded on a UV-vis spectrometer (Puxi, UV-1901).

2.3 Photocatalytic activity

The photocatalytic degradation of Rhodamine B was carried out to evaluate the photocatalytic activity of the samples. Illumination was provided by a 250 W metal halide lamp (Philips) with a UV filter (λ>400 nm, transmittance > 90%) at a distance of 10 cm from the beaker and the surface area of irridiation on the reactor was 28 cm^2. Cooling was provided by an external cooling jacket and the temperature of the reaction was controlled to 25 ±2 ℃. For a typical experiment, 0.25 g catalyst was added into 250 mL solution. The mixture was stirred in the dark for 30 min to establish adsorption equilibrium between the catalyst surface and the dye molecules. The solution was then irradiated by visible light (λ>400 nm) for two hours. The initial concentration of Rhodamine B used was 10 mg/L. During irradiation, samples were withdrawn every 15 minutes. The samples were centrifuged to remove the catalyst and the supernatant was analyzed using a spectrophotometer. The peak absorbance used was λ=554 nm, and was correlated to concentration using the Beer-Lambert law and a prepared standard curve.

3 Results and discussion

3.1 Catalyst characterization

XRD was used to determine the phase structure of the samples. Fig.1 shows the XRD patterns of the H-Ag@AgCl (synthesized via hydrothermal), P-Ag@AgCl (synthesized via precipitation) and H-AgCl. The diffraction peaks (at 38.2° and 44.4°) assigned to metallic Ag are also displayed in the nanojunction

system (the inset of Fig. 1), and was found to be especially weak, indicating that Ag was poorly crystallized. The XRD patterns of the as-prepared products indicated that the H-Ag@AgCl was better crystallized than P-Ag@AgCl. Compared with H-AgCl, the XRD pattern of H-Ag@AgCl shows two additional peaks, which are indexed to the metal silver, indicate the successful formation of silver by photoreduction under visible light irradiation, causing broadening of the visible light response due to the SPR effect of Ag NPs.

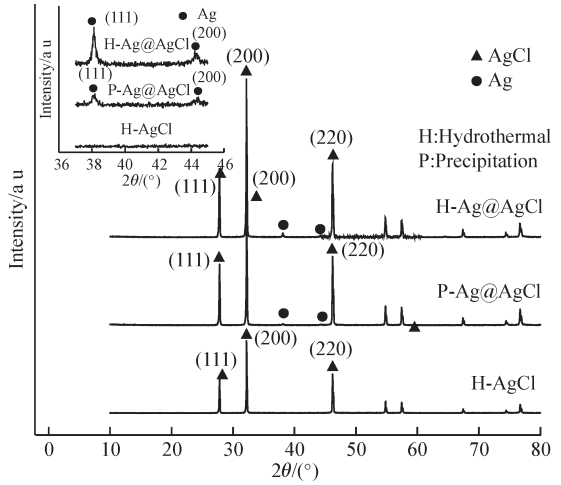

Fig.1 XRD patterns of H-Ag@AgCl, P-Ag@AgCl and H-AgCl

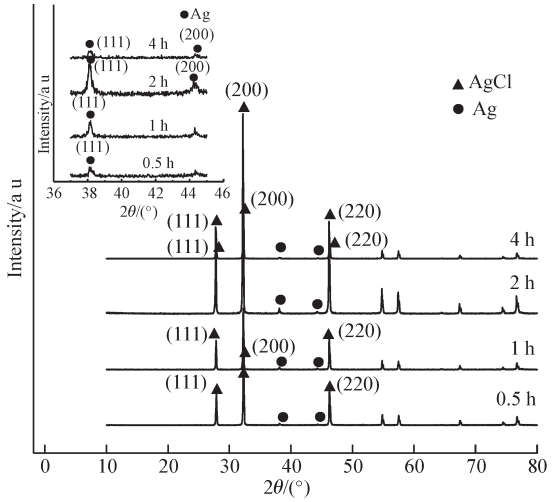

Fig.2 XRD patterns of samples prepared using various hydrothermal treatment times

Fig.2. shows a typical XRD pattern of the as-prepared product from the hydrothermal synthesis, as well as the patterns obtained for samples prepared using various treatment times. The inset in Fig.2 indicates clearly the Ag peaks at 38.2° and 44.4°. Ag@AgCl is mainly composed of AgCl and all of the peaks matched with the JCPDS standard data of AgCl (JCPDS file: 31-1238). The diffraction peaks obtained were intense and sharp, indicating that the obtained Ag@AgCl photocatalysts were well crystallized. As shown in Fig.2, the characteristic diffraction peaks for AgCl at 2θ of 27.8°, 32.2°, and 46.2° were attributed to the (111), (200), and (220) crystal planes of AgCl crystal, while the peaks at 38.2° and 44.4° were attributed to the small quantity of residual Ag. From the diffraction patterns obtained, it was found that the hydrothermal treatment time was a significant factor influencing the crystallinity. With increasing treatment time, the crystallinity of Ag@AgCl increased up to a point. However, upon exceeding an optimal treatment time, the crystallinity of Ag@AgCl was thought to be partially destroyed. This would also influence the morphology and change the specific surface area of the resulting photocatalyst.

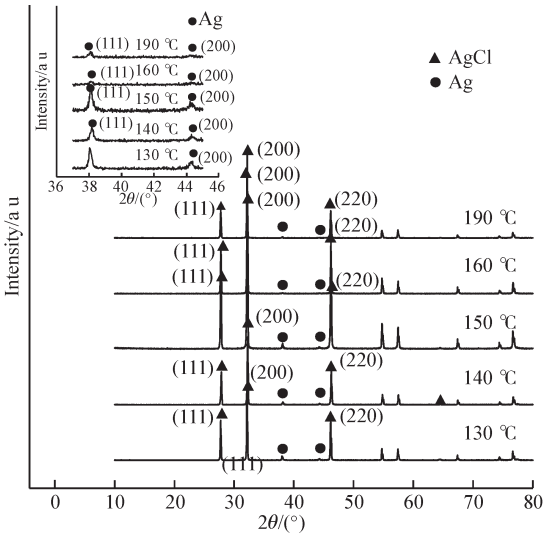

Fig.3 XRD patterns of the samples prepared at various hydrothermal treatment temperatures

Fig.3 shows a typical XRD pattern of the as-prepared product from the hydrothermal synthesis, as well as patterns obtained for samples prepared using various treatment temperatures. From the results, the cubic phase of Ag (JCPDS file: 04-0783) was seen to coexist with the cubic phase of AgCl (JCPDS file: 31-1238). The diffraction peaks obtained for all samples were intense and sharp, indicating that the Ag@AgCl photocatalysts prepared at various treatment temperatures were well crystallized. As shown in Fig.3, the characteristic diffraction peaks for AgCl at 2θ of 27.8°, 32.2°, and 46.2° were attributed to the (111), (200), and (220) crystal planes of AgCl crystal, while the peaks at 38.2° and 44.4° were attributed to the small quantity of residual Ag (the inset of Fig.3). The diffraction peak assigned to metal Ag was broad and weak, which may be a result of its low content and

small particle size on the surface of the as-prepared composite. From the diffraction patterns shown in Fig.3, the hydrothermal treatment temperature was found to be a significant factor. The increase of annealing temperature was found to result in the crystalline growth of the chlorar-gyrite phase. When the treatment temperature was 150 ℃, the best crystallinity of chlorargyrite was observed, and the cubic-type morphology was thought to be well-developed, since chlorargyrite was the dominant phase (81%).

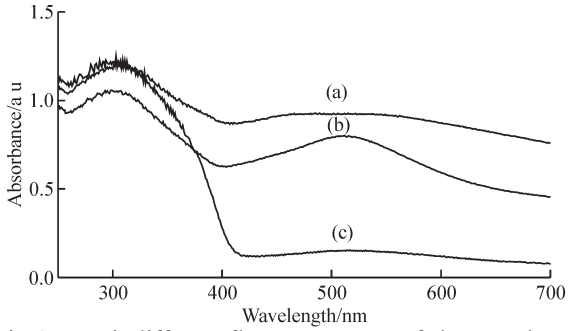

Fig.4 UV-vis diffuse reflectance spectra of photocatalysts: (a)H-Ag@AgCl; (b)P-Ag@AgCl; (c)H-AgCl

The UV-vis diffuse reflectance spectra of H-Ag@AgCl, P-Ag@AgCl and H-AgCl are shown in Fig.4. These materials were all found to exhibit a strong absorption in the UV region, a typical characteristic of silver. Both H-Ag@AgCl and P-Ag@AgCl exhibited a wide absorption ranging from 400 to 700 nm. It is interesting to find that the unreduced sample H-AgCl exhibited a characteristic absorption peak of AgCl, with the value of the absorption edge located at 400 nm. The weak absorption peak in the visible range for AgCl can be attributed to the small amount of silver nanoparticles formed under weak irradiation from the environment during preparation. In contrast to AgCl, Ag@AgCl shows a strong absorption in the visible region, attributable to the surface plasmon resonance of silver NPs deposited on AgCl particles. When the wavelength of the irradiating light is much greater than the diameter of silver NPs, the electromagnetic field across each entire silver NP is essentially uniform. With the oscillations in that electromagnetic field, the weakly bound electrons of the silver nanoparticles respond collectively, giving rise to the plasmonic state. When the incident light frequency matches the plasmonic oscillation frequency, the incident light will be absorbed, resulting in surface plasmon absorption. When the catalysts were irradiated with visible light, some Ag nanoparticles on the surface of the catalysts became larger as a result of the reduction of AgCl. Therefore, the shape and diameter of the Ag NPs obtained may have varied over a large range[18]. The absorption edge of AgCl observed in Ag@AgCl crystals was slightly blue shifted compared to that of pure AgCl particles, which may be due to a slight change in morphology and decrease in size of Ag@AgCl particles compared to the pure AgCl particles[17]. In addition, the absorbance intensity of the P-Ag@AgCl synthesized by precipitation was lower than that of H-Ag@AgCl. This indicated that the hydrothermal procedure resulted in a uniform Ag distribution on the surface of AgCl and caused the high crystallinity of Ag@AgCl.

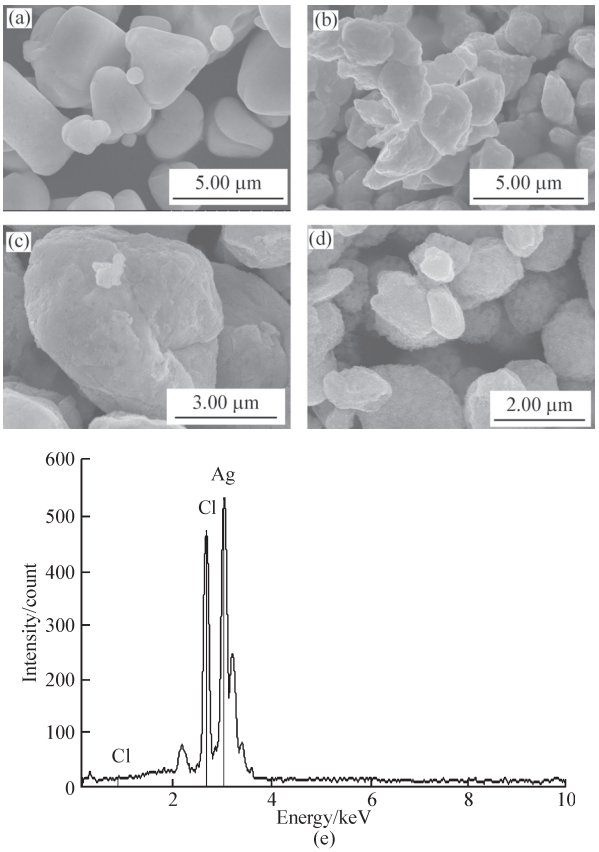

Fig.5 SEM images of photocatalyst: (a) H-Ag@AgCl; (b) H-Ag@AgCl(without CTAC); (c) H-AgCl; (d) P-Ag@AgCl; (e) corresponding EDX pattern of (a)

The morphologies of (a) H-Ag@AgCl, (b) H-Ag@AgCl (without CTAC), (c) H-AgCl and (d) P-Ag@AgCl photocatalysts were observed using SEM. Figs.5(a), (b), (c) and (d) present typical SEM images of the as-prepared photocatalyst, from which the existence of silver nanoparticles on the surface of the samples cannot be clearly identified. As shown in Fig.5(a), the Ag@AgCl photocatalyst exhibits a uniform, heart-like morphology while in Figs.5 (b), (c) and (d), the heart-like particles are in existence with

ellipsoidal ones. In addition, compared with (a) H-Ag@AgCl, (b) H-Ag@AgCl (without CTAC) shows an irregular and rough morphology. What's more, it's easy to agglomerate with each other. In this process, cationic surfactant CTAC could limit the number of nucleation sites that AgCl could grow, leading to homogeneously dispersed AgCl islands. Aside from this, CTAC could supply bromide to precipitate Ag^+ in solution; however, it should be noted that metal Ag formation occurred along with the formation of AgCl[19,20]. Fig.5 (e) shows the typical EDX spectrum obtained from H-Ag@AgCl. From the spectrum, only Ag and Cl elements were observed (copper signals appear from the copper grid), indicating the presence of AgCl and/or Ag in nanojunction system. EDX relies on the penetration depth of electrons with relatively high kinetic energy and yields the composition of the material within a region approximately 1 μm below the surface[21]. It might contain information not only due to the nanoplate surface but also due to the core of the sample clusters. Quantitative analysis of the EDX peaks obtained from Ag@AgCl yields an Ag/Cl atomic ratio of 1.2, which is close to the stoichiometric ratio.

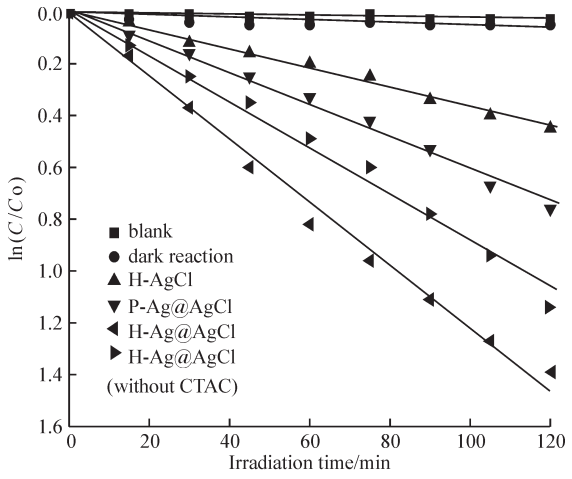

Fig.6 Comparison of photocatalytic activity for the degradation of RhB.

3.2 Photocatalytic activity for RhB degradation

The photocatalytic activity for the degradation of RhB was investigated and a comparison of the results obtained for the H-AgCl, P-Ag@AgCl, H-Ag@AgCl and H-Ag@AgCl (without CTAC) is shown in Fig.6, with the photolysis (blank) and catalysis-only (dark reaction) data for reference. The degradation was represented using the relationship between $\ln(c/c_0)$ (c_0, the initial concentration of RhB after adsorption; c, the concentration of RhB after photoirradiation) and irradiation time, and was found to be linear, indicating that the photocatalytic degradations of RhB follow first-order kinetics in all cases. A comparison of the final degradation achieved using the photocatalysts synthesized by various methods is given in the inset. The activities of the samples decrease in the orders of H-Ag@AgCl (74.51 %), H-Ag@AgCl (without CTAC) (67 %), P-Ag@AgCl (52.5 %) and H-AgCl (36.22 %). No obvious degradation was observed during the blank test and dark test, indicating that the dye was stable under visible light irradiation and that the absorption of RhB had a negligible impact on reaction after the adsorption-desorption equilibrium. The H-Ag@AgCl(150 ℃, 2 h) sample exhibited the highest decolorization rate after irradiation for 2 hours. It was found that the catalyst H-Ag@AgCl showed higher photocatalytic activity than the catalysts prepared by precipitation and prepared without CTAC, which is in accordance with their respective crystallinities and band gap energies observed. And CTAC influence on the morphology and dispersion of the photocatalyst can also affect the activity of the photocatalyst. The H-AgCl photocatalyst showed limited photocatalytic activity at the beginning of the photodegradation of RhB, since H-AgCl was not likely to produce photoelectrons and holes due to its band gap at 3.25 eV. The photocatalytic activity of the reduced H-Ag@AgCl was observed to be higher due to the generation of Ag nanoparticles on the surface of AgCl.

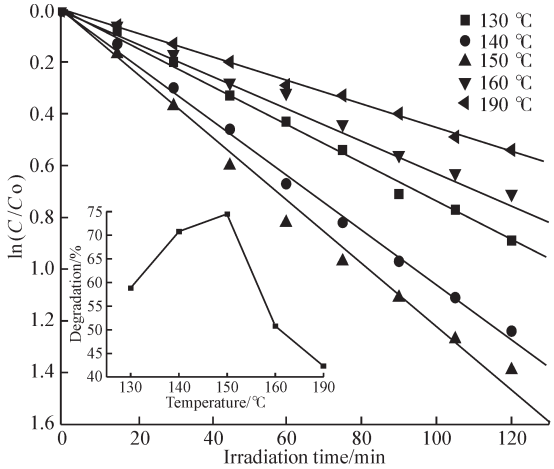

Fig.7 Infuence of the hydrothermal treatment temperature on the photodegradation rate of RhB

The effect of hydrothermal treatment temperature on the photocatalytic activity was investigated and the results are presented in Fig.7. A comparison of the final degradation achieved using the catalysts prepared at various treatment temperatures is shown in the inset. The hydrothermal treatment temperature was found to have a significant effect on the degradation rate. As shown, the relative activity observed was, in decreasing

order, 190 ℃ Ag@AgCl, 160 ℃ Ag@AgCl, 130 ℃ Ag@AgCl, 140 ℃ Ag@AgCl, 150 ℃ Ag@AgCl. Among the Ag@AgCl samples prepared at different hydrothermal treatment temperatures, the photocatalyst treated at 150 ℃ exhibited the highest photocatalytic activity and 74.51 % RhB was degraded after 2 hours of irradiation. From the trend in activity observed, it was found that an increase in temperature could improve the Ag@AgCl crystallinity, which was beneficial for the reaction. However, when the temperature used was too high, the particle diameter was thought to increase markedly, significantly influencing the separation and transfer of the photoelectrons and the holes, reducing the overall photocatalytic activity observed.

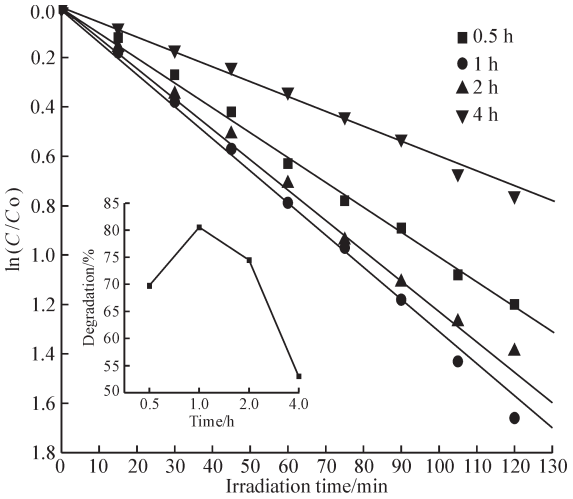

Fig.8 Influence of the hydrothermal treatment time on the photodegradation rate of RhB

Fig.8 shows the photocatalytic activity of the Ag@AgCl prepared using various hydrothermal treatment times. As shown in the inset of Fig.8, the relative photoactivity observed was found to be, in decreasing order, 4 h Ag@AgCl, 0.5 h Ag@AgCl, 2 h Ag@AgCl, 1 h Ag@AgCl. Among the Ag@AgCl photocatalysts prepared, the sample treated for 1 h exhibited the highest photocatalytic activity and 80.56 % RhB was degraded after irradiation for 2 hours. The hydrothermal treatment time was found to be a significant factor influencing the photodegradation rate. With an increase in time, the crystallinity of Ag@AgCl increased, which was favorable for the reaction. However, upon prolonged exposure, the morphology was thought to change markedly, significantly influencing the specific surface area and consequently reducing the photocatalytic activity.

The effect of dosage on the degradation of RhB was investigated in the range of 0.5-2.0 g/L, as shown in Fig.9. As expected, the degradation activity was enhanced with increasing catalyst dosage, characteristic of heterogeneous photocatalysis[22]. The lowest final degradation achieved was 38.54 % using a dosage of 0.5 g/L, while the highest degradation of 99.13 % was achieved using 2.0 g/L. The increased Ag@AgCl dosage provided more active centers due to the increment of the surface area, causing an increase in the photocatalytic degradation rate.

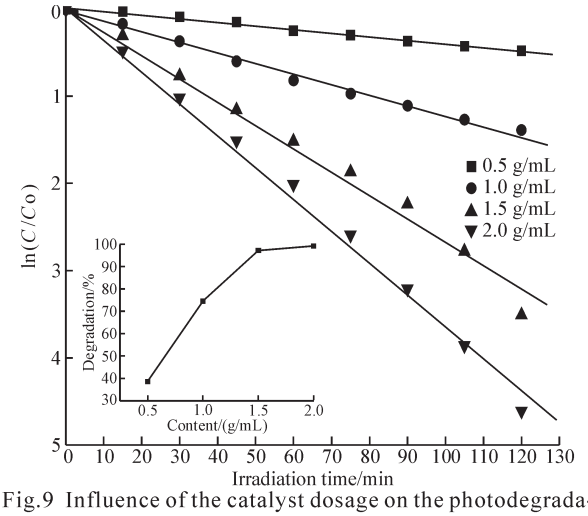

Fig.9 Influence of the catalyst dosage on the photodegradation rate of RhB

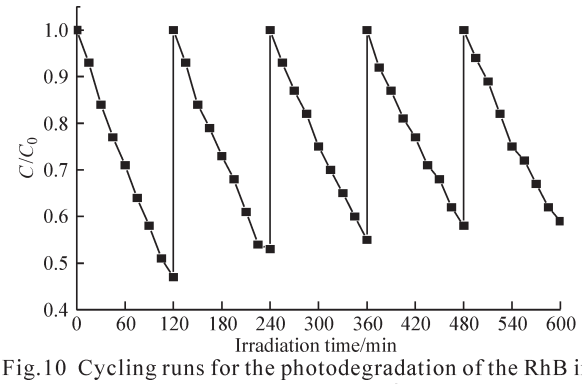

Fig.10 Cycling runs for the photodegradation of the RhB in the presence of Ag@AgCl (150 ℃,1 h) under visible light. Experimental condition: RhB concentration (10 mg/L, 250 mL), catalyst concentration (1 g/L)

The stability of a practical photocatalyst is as important as its photocatalytic activity. The stability of the Ag@AgCl (150 ℃,1 h) nanojunction system was studied through the degradation of RhB under visible-light irradiation. After five cycles of photodegradation, the Ag@AgCl nanojunction did not show a significant loss of photocatalytic activity. It should be noted that the Ag@AgCl was easily recycled by simple filtration without any treatment in these experiments and the catalyst remained stable during the photocatalytic reaction. Therefore, the present Ag@AgCl nanojunction photocatalyst is an effective and stable photocatalyst.

4 Mechanism analysis

The electronic structures of visible-light-responsive Ag@AgCl have been widely studied by researchers. Based on this discussion, the photocatalytic process using the Ag@AgCl nanojunction system can be proposed as shown in Fig.11. AgCl has a direct band gap of 5.6 eV and an indirect band gap of 3.25 eV, which has a limited utilization of visible light. Ag@AgCl is stable and efficient under visible light due to the surface plasmon resonance (SPR) of silver metal nanoparticles. The photocatalytic reaction is initiated by the absorption of visible-light photons with energy equal to or higher than the band-gap in either AgCl or Ag, which results in the creation of photogenerated holes in its valence band (VB) and electrons in its conduction band (CB). The Ag@AgCl visible light photocatalytic activity can be explained by the following mechanism. In the photocatalytic system, since the energy level of Ag is above the VB of AgCl, VB-holes (AgCl) also easily flow into metal Ag (electron transfer: Ag^{-}>AgBr), which is faster than the electron–hole recombination between the VB and CB of AgCl. Additionally, a photon could be absorbed by the metallic silver nanoparticles under visible light irradiation. Due to the dipolar character of the surface plasmon state of Ag nanoparticles, the absorbed photon would then be efficiently decomposed into an electron and a hole[12,17], such that an electron is transferred to the surface of the Ag nanoparticle farthest away from the Ag@AgCl interface, and a hole to the surface of the AgCl particle bearing the Ag. The holes are transferred to the AgCl surface corresponding to the oxidation of Cl^{-} to Cl^{0}, which should be able to oxidize RhB dye and become Cl^{-} again[23], and the Ag^{+} recombines with Cl^{-} to regenerate AgCl, so the Ag@AgCl can remain stable without deterioration. In general, photogenerated electrons are expected to be trapped by O_2 in the solution to form superoxide ions (O_2^{-}) and other reactive oxygen species[24,25]. In summary, the Ag@AgCl plasmonic photocatalyst is an efficient and stable photocatalyst under visible light.

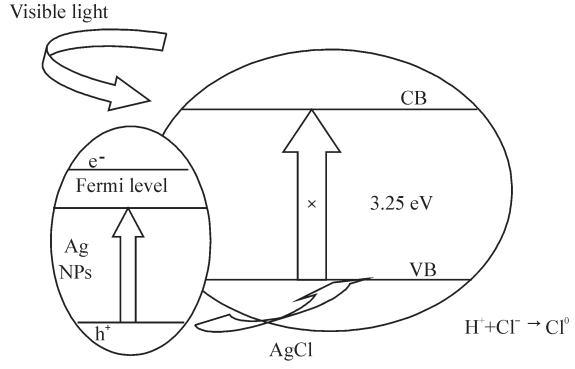

Fig.11 Photocatalytic scheme of the Ag@AgCl nanojunction system

5 Conclusions

In summary, Ag@AgCl plasmonic photocatalyst, synthesized by the simple hydrothermal photoreduction method, was found to be a novel visible light driven photocatalyst for the degradation of RhB. The Ag@AgCl particles exhibited strong absorption in visible light region because of the plasmon resonance of silver NPs on the surface of AgCl particles and the prepared photo-catalyst possessed a high photocatalytic activity. The high stability observed could be attributed to the strong absorption of silver NPs in the visible light region, so that the photogenerated electrons in Ag@AgCl were absorbed by the silver NPs rather than being transferred to the Ag^{+} of the AgCl lattice. The hydrothermal time and temperature were found to significantly affect the photodegradation of RhB. The effect of catalyst dosage was studied, and the activity increased with increasing dosage It is believed that the as-prepared Ag@AgCl will be a promising nanostructured visible light photocatalyst for future use in environmental remediation.

References

[1] Akhavan O. Graphene Nanomesh by ZnO Nanorod Photocatalysts[J]. *ACS Nano*., 2010, (4): 4 174-4 180

[2] Zhang J, Xu Q, Feng Z C. Importance of the Relationship Between Surface Phases and Photocatalytic Ac-tivity of TiO_2[J]. *Angew. Chem. Int. Ed*., 2008 (47): 1 766-1 769

[3] Esswein A J, Nocera D G. Hydrogen Production by Molecuar Photocatalysis[J]. *Chem. Rev*., 2007, (107): 4 022-4 047

[4] Deng Z, Chen M, Gu G. A Facile Method to Fabricate ZnO Hollow Spheres and Their Photocatalytic Prop-erty[J]. *Phys. Chem. B*, 2008(112): 16-22

[5] Chen X, Mao S S. Titanium Dioxide Nanomaterials: Synthesis, Properties, Modifications, and Applica-tions[J]. *Chem. Rev.*, 2007(107): 2 891-2 899

[6] Zhou X M, Liu G, Yu J G. Surface Plasmon Resonance-Mediated Photocatalysis by Noble Metal-Based Composites Under Visible Light [J]. *J. Mater. Chem*., 2012(22): 21 337-21 354

[7] Yu J G, Dai G P, Huang B B. Fabrication and Characterization of Visible-Light-Driven Plasmonic Photo-catalyst Ag/AgCl/TiO_2 Nanotube Arrays [J]. *Phys. Chem*., 2009 (113): 16 394-16 401

[8] Papavassiliou G C. Optical Properties of Small Inorganic and Organic Metal Particles[J]. *Prog. Solid State Chem*., 1979(12): 185-271

[9] Bi Y P, Ye J H. Heteroepitaxial Growth of Platinum Nanocrystals

on AgCl Nanotubes Via Galvanic Re-placement Reaction[J]. *Chem. Commun*., 2010, (46): 1 532-1 534

[10] Wang P, Huang B B, Lou Z Z. Synthesis of Highly Efficient Ag@AgCl Plasmonic Photocatalysts with Various Structures[J]. *Chem. Eur. J*. 2010(16): 538-544.

[11] Wang P, Huang B B, Lou Z Z. Highly Efficient Visible Light Plasmonic Photocatalyst Ag@Ag(Br.I)[J]. *Chem. Eur. J*., 2010(16): 538-44

[12] Zhu Y Q, Liu H L, Yang L B. Study on the Synthesis of Ag/AgCl Nanoparticles and Their Photocatalytic Properties[J]. *Mater. Res. Bull*., 2012 (47): 3 452-3 458

[13] Xu H, Li H M, Xia J X, *et al.* One-Pot Synthesis of Visible-Light-Driven Plasmonic Photocatalyst Ag/AgCl in Ionic Liquid[J]. *Mater. Interfaces*, 2011 (3): 22-29

[14] Yang Y Q, Zhang G K, Xu W. Facile Synthesis and Photocatalytic Properties of Ag-AgCl-TiO_2/Rectorite Composite[J]. *J. Colloid Interface Sci*., 2012 (376): 217-223

[15] Kuai L, Geng B, Chen X. Facile Subsequently Light-Induced Route to Highly Eficient and Stable Sunlight-Driven Ag-AgBr Plasmonic Photocatalyst[J]. *Langmuir*., 2010 (26): 18 723-18 727

[16] Lou Z Z, Huang B B, Qin X Y. One-Step Synthesis of AgBr Microcrystals with Different Morphologies by ILs-Assisted Hydrothermal Method[J]. *Cryst. Eng. Comm*., 2011, (13): 1 789-1 793

[17] Liao J, Zhang K, Wang L J. Facile Hydrothermal Synthesis of Heart-Like Ag@AgCl with Enhanced Visible Light Photocatalytic Performance[J]. *Mater. Lett.*, 2012 (83): 136-139

[18] Guo J F, Ma B W, Yin A Y. Highly Stable and Efficient Ag/AgCl@ TiO_2 Photocatalyst: Preparation, Charac-terization, and Application in the Treatment of Aqueous Hazardous Pollutants[J]. *J. Hazard. Mater*., 2012 (211-212): 77-82

[19] Hu C, Lan Y Q, Qu J H. Ag/AgBr/TiO_2 Visible Light Photocatalyst for Destruction of Azodyes and Bacte-ria[J]. *Phys. Chem. B*, 2006 (110): 4 066-4 072

[20] Elahifard M R, Rahimnejad S, Haghighi S. Apatite-Coated Ag/AgBr/ TiO_2 Visible-Light Photocatalyst for Destruction of Bacteria[J]. *J. Am. Chem. Soc*., 2007 (129): 9 552-9 553

[21] Tierno P, Goedel W A. Using Electroless Deposition for the Preparation of Micron Sized Polymer/Metal Core/Shell Particles and Hollow Metal Spheres[J]. *J. Phys. Chem. B*., 2006 (110): 3 043-3 050

[22] Wang D S, Duan Y D, Luo Q Z. Visible Light Photocatalytic Activities of Plasmonic Ag/AgBr Particles Synthesized by a Double Jet Method [J]. *Desalination*, 2012 (87): 94-96

[23] Xu H, Li H M, Xia J X. One-Pot Synthesis of Visible-Light-Driven Plasmonic Photocatalyst Ag/AgCl in Ionic Liquid[J]. *Mater. Interfaces*, 2011 (3): 22-29

[24] Soni S S, Henderson M J, Bardeau J F. Visible-Light Photocatalysis in Titania-Based Mesoporous Thin Films[J]. *Adv. Mater*., 2008 (20): 1 493-1 498

[25] Hoffmann M R, Martin S T, Choi W. Environmental Applications of Semiconductor Photocatalysis[J]. *Chem. Rev*., 1995, (95): 69-96